ORCA – Online Research @ Cardiff

The last 1 million years of the extinct genus *Discoaster*: Plio–Pleistocene environment and productivity at Site U1476 (Mozambique Channel)

Deborah N. Tangunan[a], Karl-Heinz Baumann[a,b], Janna Just[b], Leah J. LeVay[c], Stephen Barker[d], Luna Brentegani[e], David De Vleeschouwer[a], Ian R. Hall[d], Sidney Hemming[f], Richard Norris[g] and the Expedition 361 Shipboard Scientific Party[10]

[a]*University of Bremen, MARUM - Center for Marine Environmental Sciences, 28359 Bremen, Germany;* [b]*University of Bremen, Department of Geosciences, 28359 Bremen, Germany;* [c]*International Ocean Discovery Program, Texas A&M University, 1000 Discovery Drive College Station, TX 77845, USA;* [d]*School of Earth and Ocean Sciences, Cardiff University Main Building, Park Place Cardiff Wales CF10 3AT, United Kingdom;* [e]*Earth and Environmental Sciences, University of Technology Queensland Gardens Point Campus, Brisbane QLD 4000, Australia;* [f]*Lamont-Doherty Earth Observatory, Columbia University, 61 Route 9W, Palisades NY 10964, USA;* [g]*Scripps Institution of Oceanography, University of California, San Diego, 9500 Gilman Drive, La Jolla CA 92093-0244, USA;* [10]*Please see supplementary materials*

Corresponding author: tangunan@uni-bremen.de

Highlights

1. A more intensified water column mixing shown by low values of *Florisphaera profunda* index occurred at the Mozambique Channel from ~2.4 Ma, resulting in increased abundances of the upper photic zone flora indicative of nutrient-rich surface water conditions.

2. Discoasters declined with global cooling and associated enhancement of surface water productivity in the tropical Indian Ocean across the Plio-Pleistocene.

3. Ecological preference of the Plio-Pleistocene *Discoaster* species resembles that of *F. profunda*, i.e., warm and oligotrophic surface water conditions.

4. The 100-kyr and obliquity signatures suggest a NH driver of the observed variability, whereas variability at the rhythm of precession is interpreted as a tropical Pacific forcing.

The last 1 million years of the extinct genus *Discoaster*: Plio–Pleistocene environment and productivity at Site U1476 (Mozambique Channel)

Deborah N. Tangunan[a], Karl-Heinz Baumann[a,b], Janna Just[b], Leah J. LeVay[c], Stephen Barker[d], Luna Brentegani[e], David De Vleeschouwer[a], Ian R. Hall[d], Sidney Hemming[f], Richard Norris[g] and the Expedition 361 Shipboard Scientific Party[10]

[a]*University of Bremen, MARUM - Center for Marine Environmental Sciences, 28359 Bremen, Germany;* [b]*University of Bremen, Department of Geosciences, 28359 Bremen, Germany;* [c]*International Ocean Discovery Program, Texas A&M University, 1000 Discovery Drive College Station, TX 77845, USA;* [d]*School of Earth and Ocean Sciences, Cardiff University Main Building, Park Place Cardiff Wales CF10 3AT, United Kingdom;* [e]*Earth and Environmental Sciences, University of Technology Queensland Gardens Point Campus, Brisbane QLD 4000, Australia;* [f]*Lamont-Doherty Earth Observatory, Columbia University, 61 Route 9W, Palisades NY 10964, USA;* [g]*Scripps Institution of Oceanography, University of California, San Diego, 9500 Gilman Drive, La Jolla CA 92093-0244, USA;* [10]*Please see supplementary materials*

Corresponding author: tangunan@uni-bremen.de

Abstract

A detailed paleoenvironment reconstruction from the Mozambique Channel, western Indian Ocean, based on the calcareous nannoplankton assemblages was conducted for the interval between 2.85 and 1.85 Myr. This study covers the period during which the successive extinction of the last five species of discoasters occurred. New productivity data obtained from the abundances of the *Discoaster* species (*Discoaster brouweri*, *D. triradiatus*, *D. pentaradiatus*, *D. surculus*, and *D. tamalis*) and other indicative calcareous nannoplankton taxa showed abundance variations, which were at paced with the 100, 41, and 23 kyr astronomical periodicities. A shift in the productivity and water-column stratification proxies occurred at ~2.4 Ma, after the onset of the Northern Hemisphere glaciation. Here we propose that the variability recorded at International Ocean Discovery Program Site U1476 reflects the interplay between forcing associated with warm tropical Pacific and cold southern ocean influences. The former is shown by consistent occurrence of warm water taxa (*Calcidiscus leptoporus*, *Oolithotus* spp., *Rhabdosphaera clavigera*, *Syracosphaera* spp., *Umbellosphaera* spp.), typical of Indonesian Throughflow surface waters. On the other hand, the occurrence of *Coccolithus pelagicus* indicates the influence of cold, nutrient-rich sub-Antarctic surface waters. A more mixed water column initiated at ~2.4 Ma, and a consequent productivity increase led to the gradual reduction of the *Discoaster* species, until their extinction at 1.91 Ma. This period was characterized by the low values of the *Florisphaera profunda* index and high abundances of upper photic zone flora, indicative of nutrient-rich surface water

42   conditions. High productivity at the location during this period could have also been amplified
43   by localized upwelling events driven by the Mozambique Channel eddies.
44

1 Introduction

48   Major climatic variability during the middle part of the Pliocene was first proposed by
49   Shackleton et al. (1984) to have triggered the onset of the Northern Hemisphere (NH)
50   glaciation. Numerous studies have corroborated this suggestion on the basis of
51   paleontological, sedimentological and geochemical records of long climate archives (e.g.,
52   Ravelo et al., 2004; Clemens et al., 1996; Christensen et al., 2017). Much of the evidence for
53   this consensus derive from stable carbon and oxygen isotope ($\delta^{18}O$ and $\delta^{13}C$) data measured
54   on planktonic and benthic foraminifera (e.g., Raymo et al., 1992; Clemens et al., 1996; Ravelo
55   et al., 2004), suggesting the significance of this phenomenon in the evolution of the Plio-
56   Pleistocene climate. This extreme climatic variability was coupled with global-scale variations
57   in the sea surface temperature (SST) (Clemens et al., 1996) and associated changes in
58   nutrient availability, which could have created a complex oceanographic regime, which in turn
59   controlled plankton distribution in the photic layer. Previous studies suggested that during the
60   late Pliocene (~3 to 2.5 Myr), a shift in marine productivity between the high latitudes and the
61   mid- to low latitudes occurred (e.g., Sarnthein and Fenner, 1988; Bolton et al., 2011). Low
62   values of biogenic silica, $CaCO_3$, organic carbon, and alkenone accumulation in marine
63   sediments from high latitude regions and high values in the mid- to low latitudes were
64   recorded, suggesting a more productive mid- to low latitude oceans during this time period.
65   These findings have important implications for Plio-Pleistocene climate since marine biological
66   productivity is a key component in the global biogeochemical cycles. Thus studies focusing
67   on the long-term trends in biological responses to climatic variations are essential in
68   understanding the interplay between the local atmospheric processes and ocean circulation
69   over several glacial/interglacial cycles, which is an essential prerequisite in modeling the
70   present and even future climate scenarios.
71
72   One of the major contributors to marine primary production, that also plays a key role
73   in both the biological and carbonate pumps are calcareous nannoplankton (nannofossils), a
74   group of single-celled, marine haptophyte algae. These organisms are one of the dominant
75   calcifying plankton groups in the oceans (e.g., Friedinger and Winter, 1987; Westbroek et al.,
76   1993) and within the fossil record, form a major part of its deep-sea sediments (e.g., Flores et
77   al., 1999; Beaufort et al., 2001; Rogalla and Andruleit, 2005). Calcareous nannoplankton live

78   in the photic layer where light intensity is strong enough to carry out photosynthesis and the

79   nutrient levels are suitable for its growth. The temporal and spatial distributions of calcareous

80   nannoplankton are controlled by latitude (light levels), ocean currents, and the ambient upper

81   ocean nutrient content, salinity, and temperature profiles of the underlying water masses

82   (Winter et al., 1994). They are sensitive to variations in water column characteristics

83   (stratification/mixing), making these organisms potentially ideal recorders of past

84   environmental conditions.

85

86   The Plio-Pleistocene is a significant time interval in calcareous nannoplankton

87   evolution history because of the recorded decrease in diversity during this time interval (Bown

88   et al., 2004; Aubry, 2007). High frequency variability in glacial/interglacial temperatures

89   occurred during this interval, with the Pleistocene exhibiting greater variance compared to the

90   late Pliocene (Ravelo et al., 2004; Lisiecki and Raymo, 2005; De Vleeschouwer et al., 2017).

91   The gradual cooling during the transition from the warm Pliocene to the cold Pleistocene

92   (Ravelo et al., 2004) was proposed by Aubry (2007) to have driven the Pliocene

93   nannoplankton turnover and subsequent extinction events. The extinct genus *Discoaster* is

94   one of the nannoplankton groups that were affected by these extreme climatic fluctuations and

95   transition. *Discoaster* exhibited a fairly continuous evolutionary development from their first

96   occurrence in the late Paleocene (60 Ma) to the extinction of the last species toward the end

97   of the Gelasian stage (1.93 Ma). Previous studies have suggested that the inception of the

98   NH glaciation during the Pliocene (Shackleton et al., 1984; Raymo et al., 1992; Clemens et

99   al., 1996) led to the successive disappearance of the *Discoaster* species (e.g., Backman and

100 Pestiaux, 1987; Chapman and Chepstow-Lusty, 1997). The successive extinction of species

101 belonging to this group until its complete demise from the geologic record thus reflects its

102 sensitivity to changes in environmental and oceanographic conditions. While these extinction

103 events are widely documented (e.g., Bukry, 1971; Chepstow-Lusty et al., 1989; Chapman and

104 Chepstow-Lusty, 1997; Raffi et al., 2006; Browning et al., 2017), our knowledge of the

105 ecological preference of the *Discoaster* species and the environment that they lived in before

106 they disappeared is still limited (e.g, Bukry, 1971; Haq and Lohmann, 1976; Aubry, 1998;

107 Schueth and Bralower, 2015). For instance, the reported diachronous occurrences (Raffi et

108 al., 2006; Schueth and Bralower, 2015) of its member taxa in different ocean basins suggest

109 that the *Discoaster* extinction cannot be explained by variations in SST alone (e.g., Chepstow-

110 Lusty et al., 1989; Chapman and Chepstow-Lusty, 1997), but is likely a result of a combination

111 of complex environmental parameters (Schueth and Bralower, 2015). There is a general

112 agreement that discoasters have an affinity for warm and oligotrophic water based on

113 assemblage analysis and geochemical evidence (Aubry, 1998; Minoletti et al., 2001; Bralower,

114 2002; Schueth and Bralower, 2015), although their depth habitat is still poorly understood. In

Here we investigated the temporal distribution of the last five species of this group (*D. tamalis*, *D. surculus*, *D. pentaradiatus*, *D. triradiatus*, *D. brouweri*) in the westernmost Indian Ocean using sediments from Site U1476 (Mozambique Channel) collected during the International Ocean Discovery Program (IODP) Expedition 361 – Southern African Climates (**Fig. 1**) (Hall et al., 2017b) to reconstruct how the environment and productivity conditions changed toward the end of this lineage. Site U1476 consists of a continuous Plio-Pleistocene sequence of foraminifera-rich or foraminifera-bearing nannofossil ooze (Hall et al., 2017b) and thus offers an exceptional opportunity for high-resolution paleoenvironment and productivity reconstructions. Together with a detailed Plio-Pleistocene calcareous nannofossil biostratigraphy at this site, we present here new records of productivity from the abundances of *Discoaster* species and compare our results with the downcore abundance record of the extant taxon *F. profunda*, a widely used productivity proxy, and to other calcareous nannoplankton taxa with established ecological preferences.

2 Site U1476 and oceanographic setting

Site U1476 lies on the Davie Ridge, a bathymetric high in the Mozambique Channel, between the African continent and Madagascar. The site is located at the northern entrance of the Mozambique Channel (15°49.25′S; 41°46.12′E; **Fig. 1**) at a water depth of 2165 m (Hall et al., 2017b). The study area is presently influenced by the seasonally reversing monsoon winds (boreal summer and winter), induced by the migration of the Intertropical Convergence Zone, with rainfall maxima during the boreal winter (Hastenrath et al., 1993). The sea surface currents in the western Indian Ocean are in turn driven by the monsoon and the semi-annual inter-monsoon trade winds (Indian Ocean equatorial westerlies). The surface waters at Site U1476 are fed by the South Equatorial Current (SEC) that flows westward year-round across the Indian Ocean, carrying warm and oligotrophic surface water of the Indonesian Throughflow (ITF) (Schott et al., 2009; **Fig. 1**). To the east of Madagascar, the SEC splits into two boundary currents flowing as the Northeast and Southeast Madagascar Currents (NEMC and SEMC),

151 respectively. The NEMC flows around the northern tip of Madagascar and merges with the
152 Mozambique Channel throughflow, forming a set of anticyclonic eddies (Schott and McCreary,
153 2001; Schouten et al., 2003), affecting Site U1476. The southward flowing SEMC was
154 suggested to have major implications in the Agulhas Current, the largest western boundary
155 current that transports salt and heat into the South Atlantic (Lutjeharms, 2006).

156
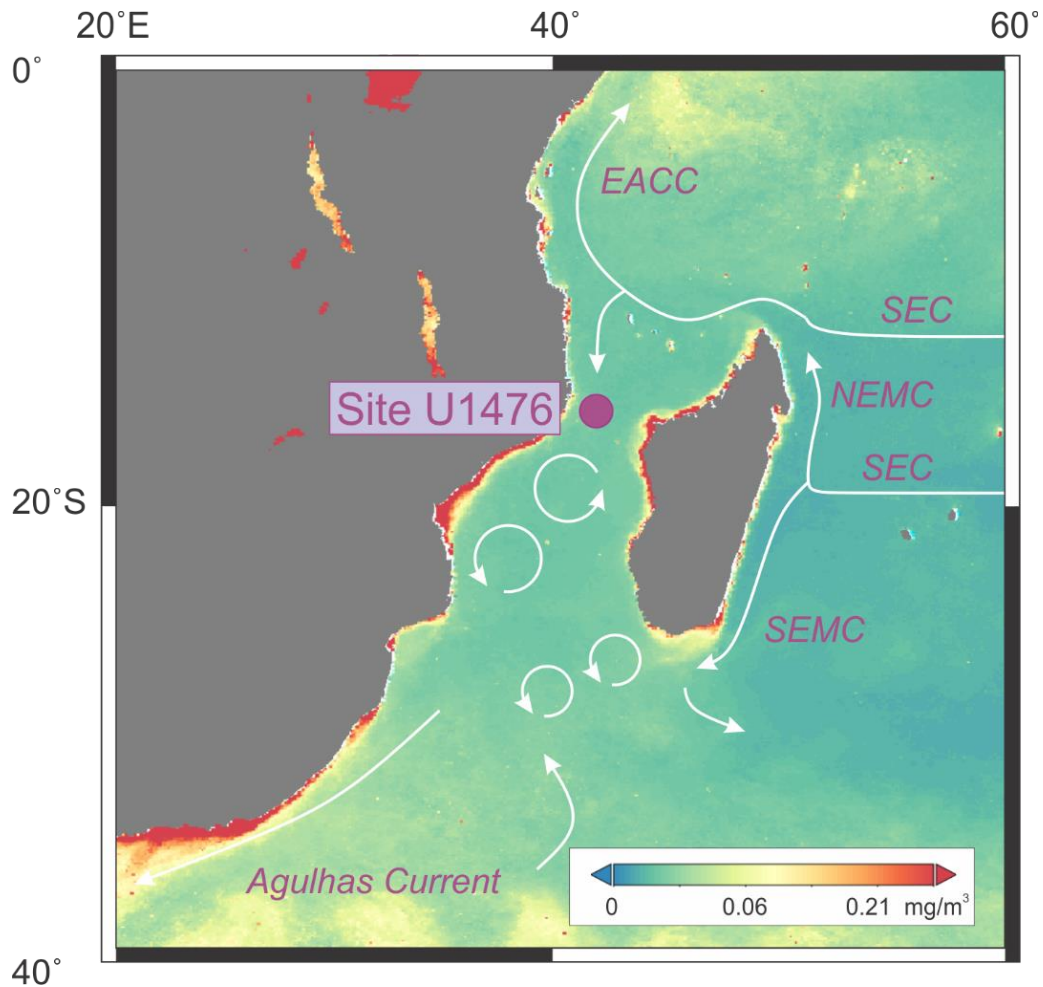
Figure 1: Location of IODP Site U1476 in the Mozambique Channel plotted on the 2010 average
chlorophyll map, with the schematic illustration of surface water circulation: East African Coastal Current
(EACC), Northeast and Southeast Madagascar Current (NEMC, SEMC); South Equatorial Current
(SEC); and South Equatorial Countercurrent (SECC). Surface water circulation was redrawn from Beal
et al. (2011). The chlorophyll map was generated using the Giovanni online data system developed and
maintained by the NASA GES DISC (Acker and Leptoukh, 2007).

164

3 Material and methods

### 3.1 Sampling strategy and age model construction

167 Samples for this study were selected between 40 and 80 m depth on the stratigraphic
168 splice, covering the Plio-Pleistocene boundary (calcareous nannofossil biozones NN15 to

NN19; 2.85 to 1.85 Myr), focusing on the interval of the *Discoaster* extinction (**Fig. 2**). Using the shipboard chronology (Hall et al., 2017b), samples were collected every ~15 cm, with a total of 269 samples and representing an average time resolution of ~5 kyr. The age model of the investigated interval was established by refining the shipboard stratigraphy by timeseries analysis and cyclostratigraphy applied on the x-ray fluorescence (XRF) Fe/Ca record of Site U1476. The Fe/Ca data series was plotted against the shipboard age model, which was based on a spline fit to the calcareous nannofossil datum events calibrated in Gradstein et al., (2012) (**Supplement Fig. S1A**). The Fe/Ca record was interpolated to make sure that the timeseries is equally spaced prior to performing the timeseries analysis to identify imprint of astronomical climate forcing (**Supplement Fig. S1B**).

We then performed a cyclostratigraphic approach on the Fe/Ca timeseries and applied a 50- to 35-kyr band-pass filter to capture an obliquity signal in the record (**Supplement Fig. S1C and S1D**). The bandpass-filtered signal was then correlated and tuned to the La2010 astronomical solution (Laskar, 2011), using the minimum Fe/Ca values and assuming low Fe/Ca during the glacial periods. Shipboard data generated from this site showed a distinct glacial-interglacial pattern of the last 1 Myr (Hall et al., 2017b), resembling the Lisiecki and Raymo (2004) benthic isotope curve. Moreover, the correlation was rather straightforward since calcareous nannofossil assessment during the expedition showed abundant and well-preserved Plio-Pleistocene specimens, which provided a reliable basis for precise chronological approximations of the datum events (**Supplement Fig. S1E**). Given the obliquity-based tuning strategy, we estimated the uncertainty on the age model to be inferior to half of an obliquity cycle, i.e., <20 kyr.

The calibrated age model yielded sedimentation rates between ~2.6 to 3.3 cm/kyr. This estimate agrees well with the average sedimentation rate of ~2.5 cm/kyr at DSDP Site 242 (Simpson and Schlich, 1974), located ~5 km southeast of the study area, and with the shipboard estimate based on the combined planktonic foraminifera and calcareous nannofossil stratigraphy (2.3 to 3.5 cm/kyr; Hall et al., 2017b). A detailed list of the identified calcareous nannofossil biostratigraphic events encountered at Site U1476 can be found in **Supplement Table S1**.
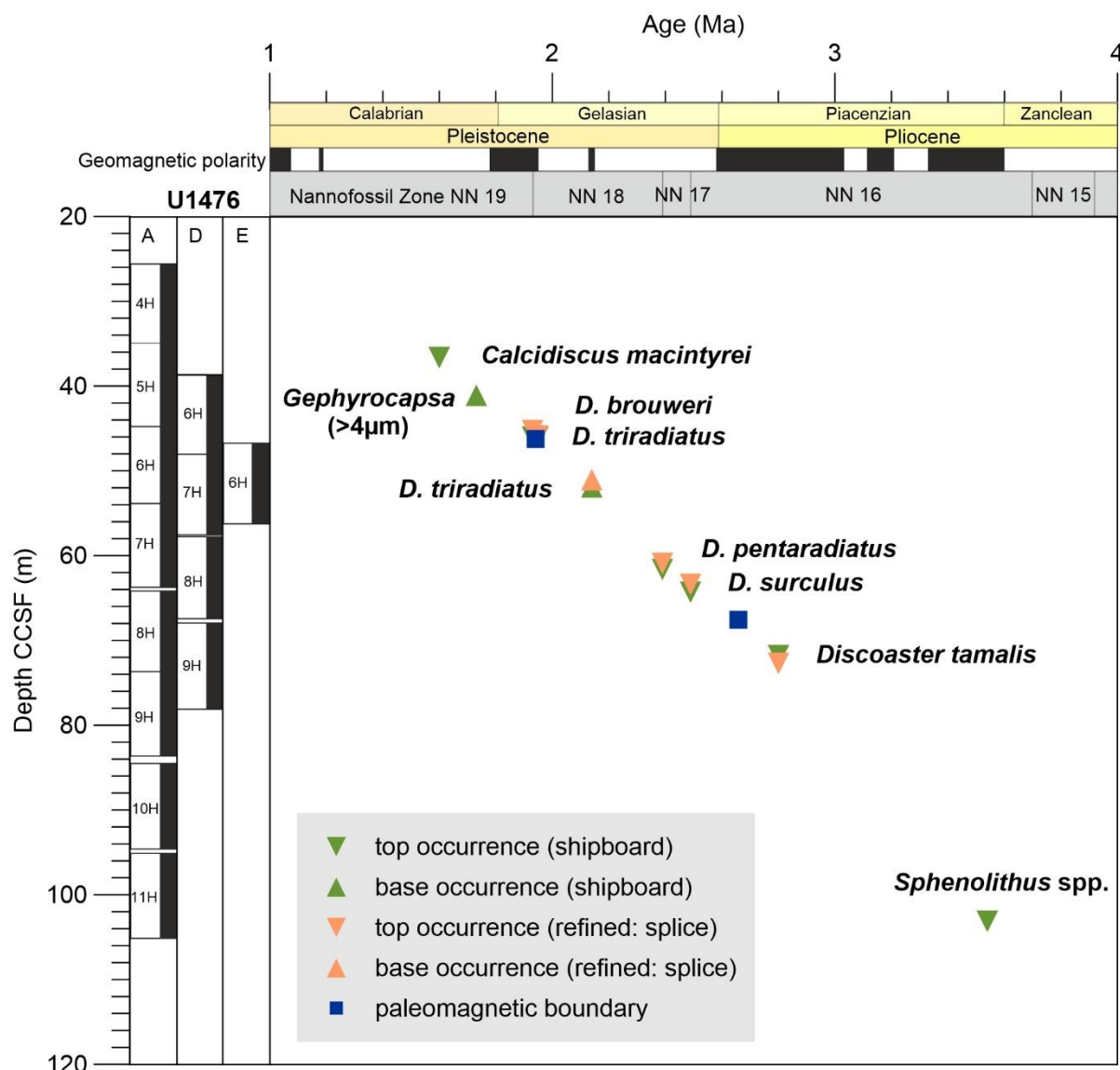
Figure 2: Age-depth relationships at Site U1476 showing the shipboard and refined occurrences of calcareous nannofossil index taxa and paleomagnetic boundaries. The five *Discoaster* datum events occurred between the late Gauss and Olduvai.

3.2 Calcareous nannofossil identification, abundance and biostratigraphy

Slides for calcareous nannofossil analysis were prepared following the drop technique of Bordiga et al. (2015). Quantitative analysis was performed with a Leica polarized light microscope under 1000 x magnification. Abundances were determined by counting at least 300 species per sample. An additional 10 to 20 fields of view (FOV) were counted to document uncommon and rare taxa. Minor reworking was observed, but when present, reworked specimens were counted separately. In each sample, the entire slide was scanned after counting to detect index taxa for refining the biostratigraphy. Supplementary smear slides were prepared for selected intervals to confirm biostratigraphic boundaries. Preservation of species

was assessed while counting using the criteria described in (Hall et al., 2017a). The zonation schemes of Martini (1971; Codes NN), Okada and Bukry (1980; Codes CN), and Backman et al. (2012; CNPL) were adopted for this study. We have initially followed the calcareous nannofossil datum events in Gradstein et al. (2012) for the preliminary age model (Hall et al., 2017b). The shipboard calcareous nannofossil biostratigraphy was then refined using the splice samples. The datum events were calibrated using the new astronomically-tuned age model and complemented by the paleomagnetic data (**Supplement Table S2 and Fig. S2)**.

Species taxonomic identification was based on Perch-Nielsen (1985), Hine and Weaver (1998), Young (1998) and the electronic guide to the biodiversity and taxonomy of calcareous nannoplankton (Nannotax 3; http://www.mikrotax.org/Nannotax3/). The conversion of nannofossil counts into absolute number of nannofossils per gram of sediment (N/g. sed.) was calculated using the equation: Nannofossil concentration = (N* A) / (f x n x W), where N = *total nannofossil counts*; A = *area of the coverslip (mm^2)*; f = *area of FOV (mm^2)*; n = *number of FOV counted*; and W = *weight of bulk dry sediment (g)*. Species diversity (Shannon index; H) was calculated using the paleontological statistical software (PAST). The Shannon index varies between 0 for populations with one species (low richness and evenness) and high values for populations consisting of several taxa, each having few individuals (high richness and evenness) (Hammer et al., 2009).

3.3 Indicative taxa for productivity and temperature

The genus *Discoaster* has been used as a warm water and low surface water productivity proxy (Backman and Pestiaux, 1987). This group is known to have an affinity for warm, oligotrophic and stratified water column conditions (Bukry, 1971; Haq and Lohmann, 1976; Aubry, 2007; Schueth and Bralower, 2015) and their extinction toward the end of the Pliocene was thought to be due to the intensified NH glaciation (Chapman and Chepstow-Lusty, 1997). In addition, cyclic patterns in the records of the Pliocene *Discoaster* taxa have been observed (e.g., Backman and Pestiaux, 1987; Chepstow-Lusty et al., 1989; Gibbs et al., 2004). Here we used the abundances of these species as both productivity and SST proxies.

The occurrence of *Coccolithus pelagicus* in the study site was also used as a SST proxy. This species is found in subarctic environments (Baumann et al., 2000) and is an indicator of cooler surface water (e.g., Marino et al., 2014). Parente et al. (2004) found this species together with high abundances of the planktonic foraminifera species *Neogloboquadrina pachyderma* (sinistral), another cold-water proxy, and interpreted their joint occurrence to be linked to the influx of subpolar waters off western Iberia during Heinrich

252 events. This species also registered distinct glacial peaks during the mid-Pleistocene
253 transition in North Atlantic sediments (Marino et al., 2011).

254

255   Transfer functions based upon the abundance of the lower photic zone (LPZ)-dwelling
256 taxon *F. profunda* have been successfully used as proxies for past changes in the
257 nutricline/thermocline depths in Quaternary sediments (e.g., Molfino and McIntyre, 1990;
258 Ahagon et al., 1993; Flores et al., 1999), and for estimation of marine primary production
259 (Beaufort et al., 1997; Beaufort et al., 2001). For this study, the estimated primary productivity
260 (EPP) expressed in grams of carbon (g C/m^2/yr) was calculated from the relative abundance
261 of this taxon using the formula: EPP = 617 - [279 * log (% *F. profunda* + 3)]. This equation,
262 however was calibrated by (Beaufort, 1996) using calcareous nannofossils from the Indian
263 Ocean core top samples and modern primary productivity generated from satellite chlorophyll
264 data by Antoine and Morel (1996). Here we use this formula by investigating Pliocene
265 sediments to test whether the EPP absolute values can be applied to ancient oceans with
266 different oceanography and biota compared to modern oceans. The EPP is used as a proxy
267 for primary productivity because in contrast to other taxa, *F. profunda* prefers to thrive in the
268 deep photic zone (Molfino and McIntyre, 1990). Hence, high abundances of *F. profunda*
269 indicate deeper nutricline/thermocline and low abundances of this species suggest otherwise.
270 The ratio of this species to smaller forms of *Gephyrocapsa* and *Reticulofenestra* (< 3µm), (*F.*
271 *profunda* index) was also used as water column stratification proxy (*F. profunda* index;
272 Beaufort et al., 1997; Beaufort et al., 2001): *F. profunda* index = *F. profunda* / (*F. profunda* +
273 small *Gephyrocapsa* + small *Reticulofenestra*). Low values of *F. profunda* index suggest a
274 more mixed water column whereas values closer to 1 indicate a more stratified water column.
275

4 Results

4.1 Extinction of *Discoaster* species in the Mozambique Channel

278   Six Plio-Pleistocene nannofossil datum events (Backman et al., 2012; Gradstein et al.,
279 2012) were recognized at Site U1476, differing by 10 to 90 kyr from the calibrated ages of
280 these events in the low and middle latitude regions in the three major oceans (South Atlantic,
281 Pacific and Indian Ocean), and the Mediterranean Sea region (**Table 1**). Taking into account
282 U1476 age model uncertainty (± 20 kyr), some of these extinction events cannot be
283 distinguished in time and thus occurred simultaneously in different ocean basins. The last
284 occurrence of *D. tamalis* (2.81 Ma) occurred 10 kyr (2.80 Ma; Lourens et al., 2004) and 50 kyr
285 (2.76 Ma; Backman et al., 2012) earlier in the study area than the reported extinction of this
286 species in the three major oceans and the Mediterranean. All of the other *Discoaster* species
287 became extinct in the Mediterranean before disappearing in the Mozambique Channel. After

the last occurrence of *D. surculus* (2.53 Ma) and *D. pentaradiatus* (2.45 Ma) in the study area, these two species became extinct in the South Atlantic 40 and 60 kyr later, respectively. The base common occurrence of *D. triradiatus* (2.13 Ma) occurred 10 kyr later in the study area than in the South Atlantic (2.14 Ma; Lourens et al., 2004) and the equatorial North Atlantic (2.14 Ma; Chapman and Chepstow-Lusty, 1997). This result is 20 kyr earlier than the recorded acme of *D. triradiatus* at Site 709 in the equatorial Indian Ocean (2.11 Ma; Chapman and Chepstow-Lusty, 1997). *Discoaster brouweri*, the last *Discoaster* species, first went extinct in the equatorial Pacific (2.06 Ma), followed by the Mediterranean (1.95 Ma; Lourens et al., 2004), the South Atlantic (1.93 Ma; Lourens et al., 2004), and finally the westernmost Indian Ocean (1.91 Ma). The extinction of this species at Site 709 is occurred with the last occurrence of *D. triradiatus* in this location (1.95 Ma; Chapman and Chepstow-Lusty, 1997). Considering the uncertainty in our age model, the extinction of the final *Discoaster* species at Site U1476 is synchronous to the recorded extinction of this group in the major ocean basins.

Table 1: Comparative global occurrence/extinction of the Plio-Pleistocene *Discoaster* compiled in Backman et al. (2012) and Gradstein et al. (2012) with the astronomically tuned datum events from this study. Calcareous nannofossil zonation scheme by Martini (1971; NN), Okada and Bukry (1980; CN) and Backman et al. (2012; CNPL) are indicated. T = top occurrence, Bc = base common occurrence.

CALCAREOUS NANNOFOSSIL DATUM EVENT	BIOZONE	CALIBRATED AGES (Ma)						
		GTS 2012 scaling	South Atlantic	Equatorial Pacific	Mediterranean	Reference	Backman et al. (2012)	western Indian Ocean (THIS STUDY) Error ± 20 kyr
T *D. brouweri*	NN19/18, CN13a/12d, CNPL 7/6	1.93	1.93	2.06	1.95	1	1.93	1.91
T *D. triradiatus*	NN18, CN12d	1.95			1.95	2		1.93
Bc *D. triradiatus*	CNPL 6	2.14	2.14		2.22	1	2.16	2.13
T *D. pentaradiatus*	NN18/17, CN12d/12c, CNPL 6/5	2.39	2.39		2.51	1	2.39	2.45
T *D. surculus*	NN17/16, CN12c/12b, CNPL 5	2.49	2.49	2.52	2.54	1	2.53	2.53
T *D. tamalis*	NN16, CN12b/12a, CNPL 5/4	2.80	2.80		2.80	1	2.76	2.81

[1]Lourens et al., 2004; [2]Berggren et al. (1995); Rio et al. (1990); Backman and Pestiaux (1987)

4.2 Nannofossil assemblage composition, preservation and diversity

A total of 35 species and species groups comprising tropical to subtropical taxa and cold water species were identified. The Plio-Pleistocene assemblage is generally well-preserved, with all the species identifiable at the species level. The assemblage at Site U1476 is dominated by *Reticulofenestra* species (13 to 63%) and *F. profunda* (2 to 59%), with alternating dominance in the record (**Fig. 3A**). This is followed by *Gephyrocapsa* spp. (up to 24%), *Discoasters* spp. (up to 17%), and *Pseudoemiliania lacunosa* (up to 15%). Other species that made significant contribution to the total assemblage are *Helicosphaera* spp., *Oolithotus* spp., *Umbilicosphaera* spp. and *Rhabdosphaera clavigera*.
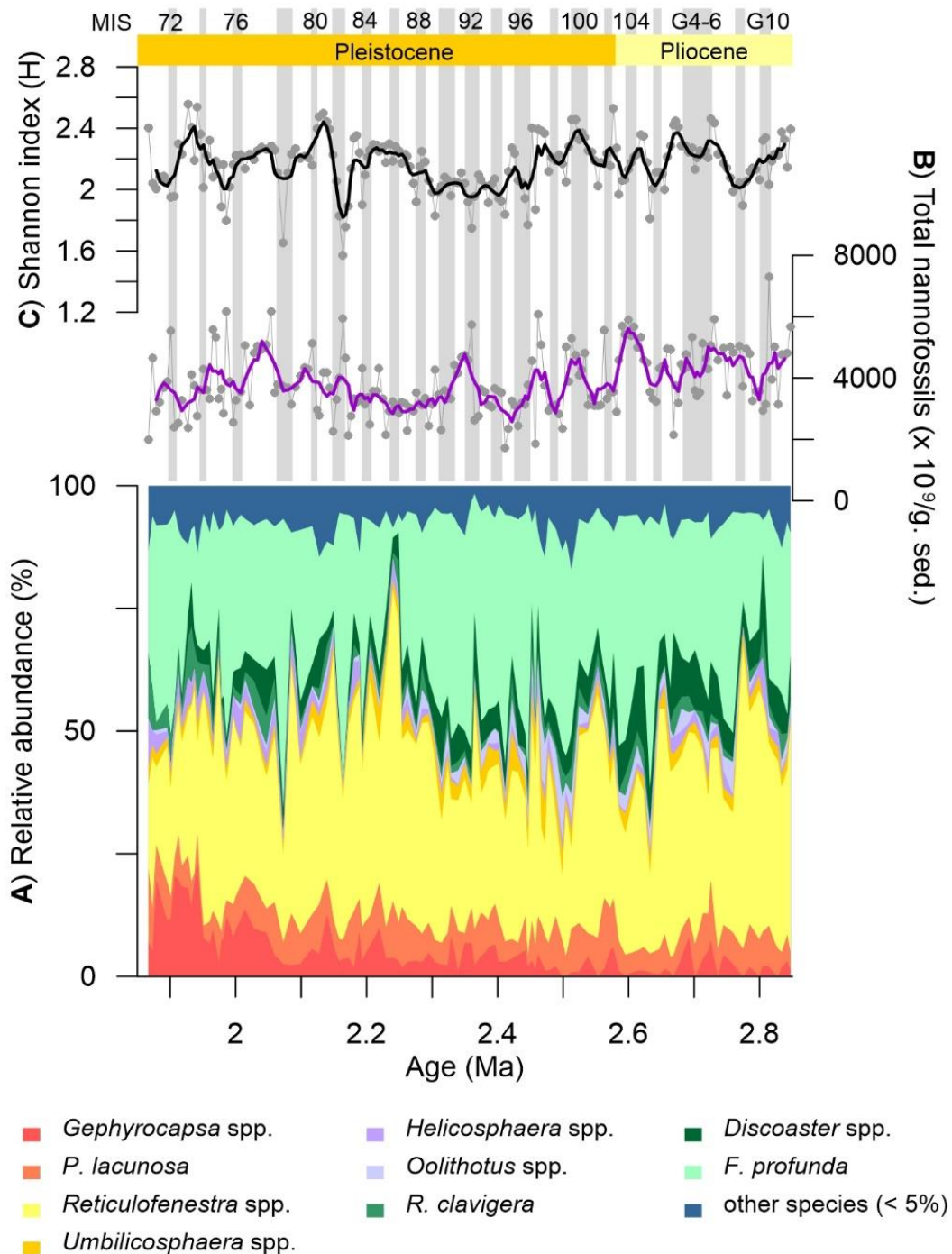
Total calcareous nannofossil absolute concentrations show highly variable patterns through the studied time interval, with total concentrations ranging from 1700 x 10^9 to 7300 x 10^9 N/g sed. (**Fig. 3B**). The Plio-Pleistocene transition (2.58 Ma) is characterized by a reduction in both the total nannofossil concentration and species diversity (**Fig. 3B** and **3C**). The Pliocene record displays a good correspondence between the total concentrations and the species diversity. From 2.31 to 2.17 Myr, consistently low total nannofossil concentrations accompanied by increased diversity occur. Total nannofossils stay at relatively similar level after the Plio-Pleistocene transition while species diversity immediately recovered.

4.3 Variations in *Discoaster* abundance

Discoaster tamalis and *D. asymmetricus* show the lowest concentrations, with maximum abundances of only up to 110 x 10^9 N/g sed. and 50x 10^9 N/g sed., respectively (**Fig. 4A** and **4B**). *Discoaster surculus* displays a relatively constant abundance from 2.85 to 2.6 Myr, gradually increases at the beginning of MIS 103 and registers a maximum concentration during this stage (290 x 10^9 N/g sed.) (**Fig. 4C**). Its abundance then progressively decreases until it completely disappears from the record at 2.53 Ma. The pattern of *D. pentaradiatus* matches *D. surculus* showing the highest concentrations during the interglacial stages G11 (430 x 10^9 N/g sed.) and MIS 103 (390 x 10^9 N/g sed.) (**Fig. 4D**). This species is the most abundant species in the investigated time interval. After 2.45 Ma, when the extinction of *D. pentaradiatus* occurred, only two members of this genus are left. Reworked specimens of this species were, however, noted above its recorded extinction (**Fig. 4D**). *Discoaster triradiatus* has a base common occurrence placed at 2.13 Ma. Maxima in abundance of this species are recorded at MIS 81 (95 x 10^9 N/g sed.), MIS 78 (150 x 10^9 N/g sed.) and MIS 74 (130 x 10^9 N/g sed.) (**Fig. 4E**). The second most abundant species in the record is *D. brouweri*, with highly variable abundance throughout the record (**Fig. 4F**). Lower concentrations of this species are recorded until 2.58 Ma, when total *Discoaster* abundance

347 is shared with other *Discoaster* taxa (*D. pentaradiatus*, *D. surculus*, *D. asymmetricus*, and *D.*
348 *tamalis*). After the extinction of *D. surculus*, *D. brouweri* dominates the *Discoaster*
349 assemblage. All of these species show declining trends toward their respective demise from
350 the Site U1476 record.

351

Figure 3: Calcareous nannofossils at Site U1476: (**A**) stack plot of all species; (**B**) total absolute nannofossil concentration per gram (g) of sediment; (**C**) Shannon diversity index (H). Glacial stages are marked by gray bars. Solid lines are calculated 5-point running average of the raw data (gray background lines) and used to highlight general patterns.

357
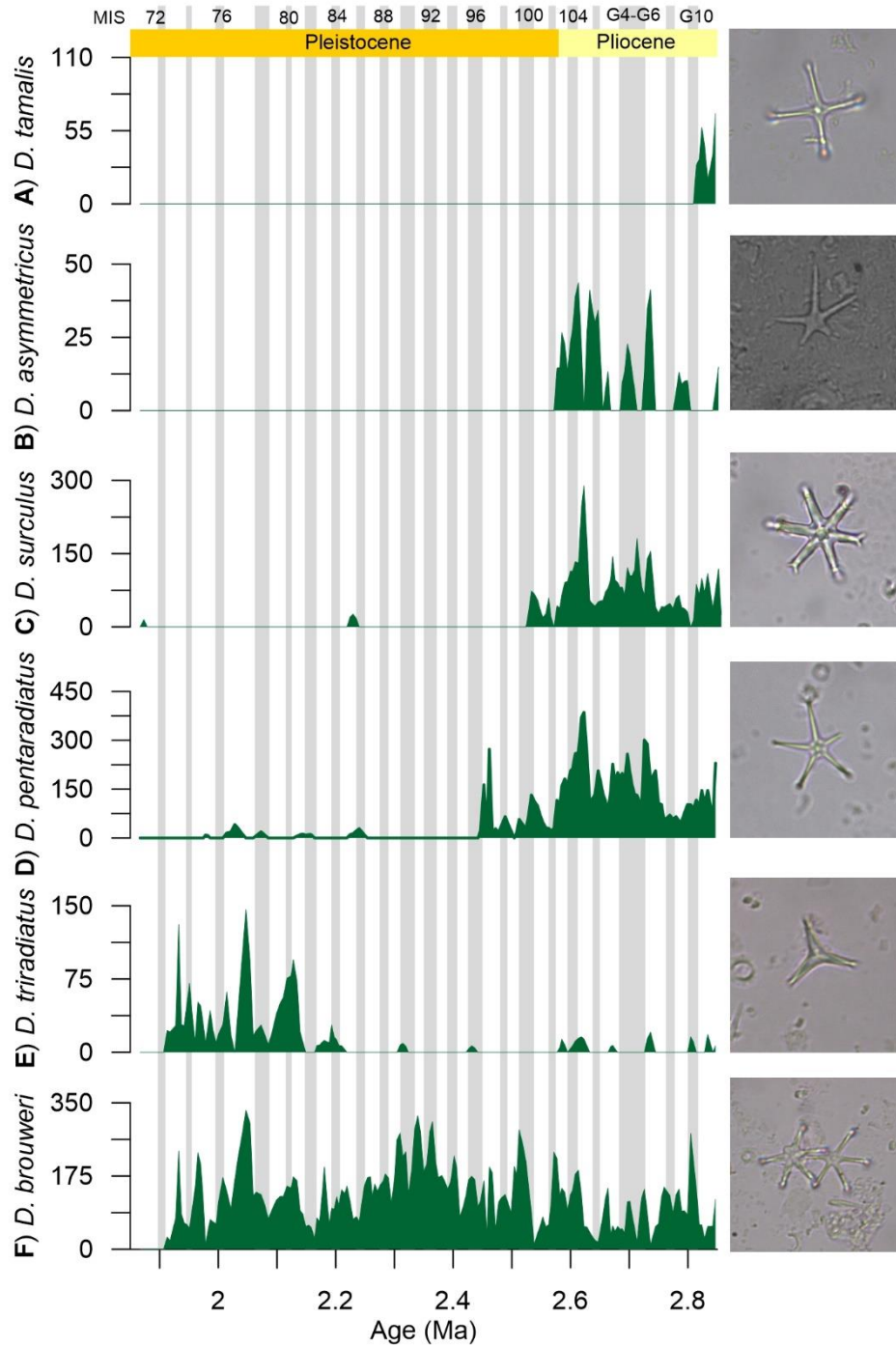
Figure 4: Absolute concentrations of the Plio-Pleistocene *Discoaster* species: (**A**) *D. tamalis*; (**B**) *D. asymmetricus*; (**C**) *D. surculus*; (**D**) *D. pentaradiatus*; (**E**) *D. triradiatus*; and (**F**) *D. brouweri*. All concentrations are expressed in number of nannofossils x 10⁹/gram of sediment. Glacial stages are marked by gray bars.

5 Discussion

### 5.1 *Discoaster* extinction and paleoenvironment during the Plio-Pleistocene

The successive extinctions of *Discoaster* species during the Plio-Pleistocene offers a well-established sequence of biostratigraphic events (Bukry, 1971; Backman and Pestiaux, 1987), including our record from Site U1476. Efforts on the refinement of these datum events have progressed over the years, including astronomical calibration (e.g., Raffi et al., 2006; Backman et al., 2012; Agnini et al., 2017). While the Pliocene nannofossil chronology is rather less studied on a global scale compared to the Miocene or Pleistocene intervals (Raffi et al., 2006), the Plio-Pleistocene *Discoaster* extinction event is widely documented. Despite the reported uncertainties in using the individual datum due to diachronous first and last occurrences of its member taxa between major oceans, there is still a general consensus that this group disappeared from the record during the transition from the warm Pliocene to the cold Pleistocene.

At Site U1476, a general reduction in the *Discoaster* abundance from 2.85 to 1.85 Myr is observed until it completely vanishes from the record at 1.91 Ma (**Fig. 5**). This record displays an opposite abundance pattern with the upper photic zone (UPZ) flora with preference for high nutrient environment, which shows an increasing abundance toward 1.85 Ma (**Fig. 5D**). This indicates the affinity of discoasters to low productivity regime, and hinting the possibility of this group to have inhabited the deep photic layer. The preference of this group to oligotrophic environment was also shown in a study by Minoletti et al. (2001), where the δ^{13}C values analyzed from the *Discoaster* fraction resemble the planktonic foraminifera record. Previous studies suggested that some *Discoaster* species prefer the LPZ, a behavior similar to *F. profunda* (e.g., Aubry, 1998; Bralower, 2002). A recent study by Schueth and Bralower (2015) confirmed this using an ecological ordination technique, where the authors suggested that *D. brouweri* and *D. pentaradiatus* favored a warm and stratified regime, with a deep nutricline. Geochemical evidence supports the first two proposed ecology of this group; however, the similarity of the discoaster δ^{18}O values to the surface water dwelling planktonic foraminifera record also indicates that they thrived in the upper photic layer (Minoletti et al., 2001). While the depth habitat of this extinct group is still controversial, our results show that discoasters inhabited warm, stratified and oligotrophic condition. And whether they thrived in the UPZ or the LPZ, if these organisms were adapted to a low nutrient regime, having a more vigorously mixed water column would be a detriment to the group even if it was abundant in the surface waters. The discoasters could have also been outcompeted by the UPZ flora,

399 which are mostly dominated by the small reticulofenestrids, a group of opportunistic taxa that

400 are abundant in nutrient-rich environment (Flores et al., 1995).

401

402 A distinct shift starting at ~2.4 Ma is observed in both the *Discoaster* and the UPZ

403 records, after the transition from the Pliocene to the Pleistocene. The increase in abundance

404 of the eutrophic UPZ flora suggests nutrient enhancement in the photic layer, which is in

405 agreement with the *F. profunda* index indicating less stratified water column conditions from

406 ~2.4 to 1.85 Myr (**Fig. 5B**). More intensified water column mixing could have shoaled the

407 nutricline leading to increase in the abundances of the UPZ flora. This shift at ~2.4 Ma

408 occurred after the onset of the Northern Hemisphere glaciation (Haug et al., 1999), and is

409 coincident with the beginning of the Arid interval (**Fig. 5**), when the fully constituted tropical

410 Indian Ocean circulation has developed (Christensen et al., 2017). Comparison with the

411 productivity record of the North Atlantic (ODP Site 982; Bolton et al., 2011) reveals a reverse

412 pattern at ~2.4 Ma, signifying a more enhanced wind-driven upwelling zones and upwelling

413 productivity in the in the low- to mid- latitudes during this period (Sarnthein and Fenner, 1999)

414 (**Fig. 5E**). On the other hand, a reduction in the *Discoaster* abundance is observed during

415 some of the extreme Early Pleistocene glacial stages, such as MIS 96, 82, 78, and 72. This

416 pattern was also recorded in the three major ocean basins (Chapman and Chepstow-Lusty,

417 1997), indicating that the global changes in the surface water conditions driven by the

418 glacial/interglacial cycles and the intensity of the NH glaciation, have controlled the abundance

419 and distribution of this particular group.

420

421 The EPP values calculated from the relative abundance of *F. profunda*, however do

422 not show a clear pattern as the other proxies discussed above (**Fig. 5E**). A relatively stable

423 pattern is observed in the EPP throughout the studied time period although higher amplitude

424 fluctuations can be observed starting at ~2.25 Ma. This shows that the EPP formula, calibrated

425 using modern samples is not an effective measure of productivity in ancient sediments.

426 Nevertheless, the reduction in water column stratification shown by the *F. profunda* index and

427 the increasing abundance of the eutrophic UPZ species indicates that gradual cooling coupled

428 with the shallowing of the nutricline/thermocline (Ravelo et al., 2004; Lawrence et al., 2013),

429 resulted in the progressive decline and subsequent demise of the discoasters (Chapman and

430 Chepstow-Lusty, 1997; Schueth and Bralower, 2015).

431
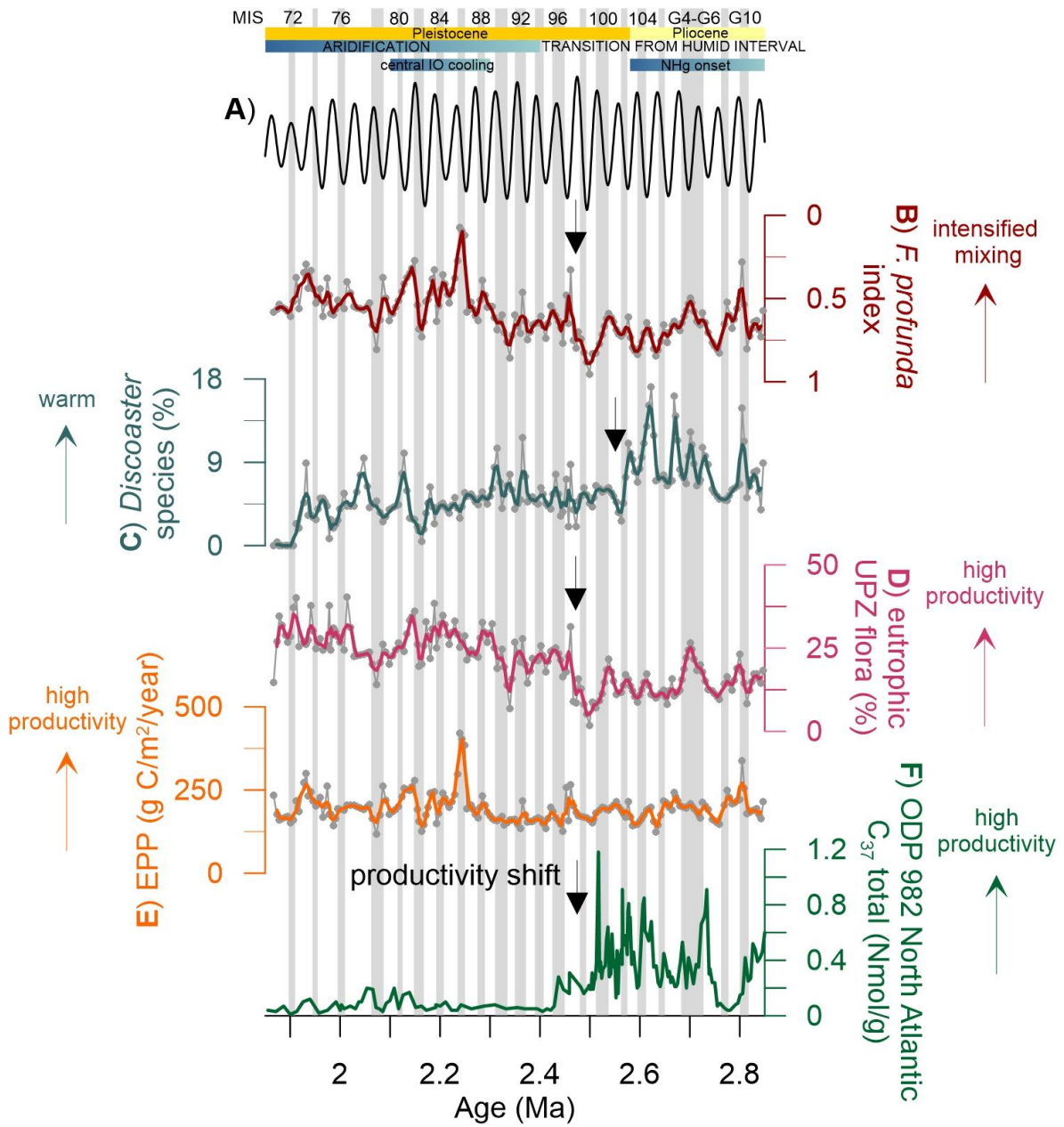
Figure 5: Site U1476 coccolithophore productivity and stratification records with major climatic and oceanographic events during the Pliocene-Pleistocene transition: (**A**) orbital obliquity sequence (Berger, 1992); (**B**) *Florisphaera profunda* index; (**C**) relative abundance of *Discoaster* spp.; (**D**) upper photic zone (UPZ) flora comprising small *Gephyrocapsa* and small *Reticulofenestra*; (**E**) estimated primary productivity (EPP) calculated from the relative abundance of *F. profunda*; and (**F**) C37 alkenones from ODP 982 (Bolton et al., 2011). Glacial stages are marked by gray bars. Atmospheric and oceanographic events at major periods of the Neogene global climate are indicated by blue horizontal bars. Solid lines are calculated 3-point running average of the raw data (gray background lines) and used to highlight general patterns.

## 5.2 Productivity fluctuations from indicative taxa

The downcore variations in individual nannoplankton species show differences in abundance patterns, with some species showing a clear trend with the implied isotope stages (**Fig. 6**). The variations in abundance of temperature and productivity indicator species suggest that a combination of environmental parameters, and not only SST, controlled the coccolithophore productivity at Site U1476 during the Plio-Pleistocene (**Fig. 6**). Despite of the scattered occurrences of *C. pelagicus* in the record, this species shows peak abundances during the glacial intervals, especially during the Early Pleistocene, which signifies the preference of this species to cold water conditions (**Fig. 6A**). Relatively stable abundances of the eutrophic UPZ group are recorded for the Pliocene sequence, and registers a major change after the transition to the Pleistocene (~2.4 Ma), where it reaches a minimum and progressively increases thereafter. The increased abundances of the eutrophic UPZ-dwelling taxa (**Fig. 6C**), indicates enriched nutrient supply in the upper photic layer (Okada, 2000). The interval from ~2.4 to 1.85 Myr is characterized by higher surface water productivity conditions, as is also shown by the increased abundances of *C. leptoporus*, another taxon with affinity for high-nutrient environments (e.g., Giraudeau, 1992; Winter et al., 1994) (**Fig. 6B**). While this species is also typified for warm conditions (Winter and Martin, 1990; Flores et al., 1999; Baumann and Freitag, 2004), its contrasting pattern with the warm water taxa (**Fig. 6F**), especially starting at ~2.2 Ma, shows that the abundances of *C. leptoporus* are not a consequence of changing SST but rather of nutrient availability in the water column. Despite the low abundances of the accessory taxa *Oolithotus* spp., *Rhabdosphaera clavigera*, *Syracosphaera* spp., and *Umbellosphaera* spp., the cumulative abundance of these species used as a warm water proxy shows distinct and regular variations in the record. The high abundances of the tropical species, such as *F. profunda*, and *C. leptoporus* coupled with the consistent occurrences of the warm water taxa (*Oolithotus* spp, *Rhabdosphaera* clavigera, *Syracosphaera* spp., and *Umbellosphaera* spp.) reflect prevalence of warm tropical conditions in the study area.

473
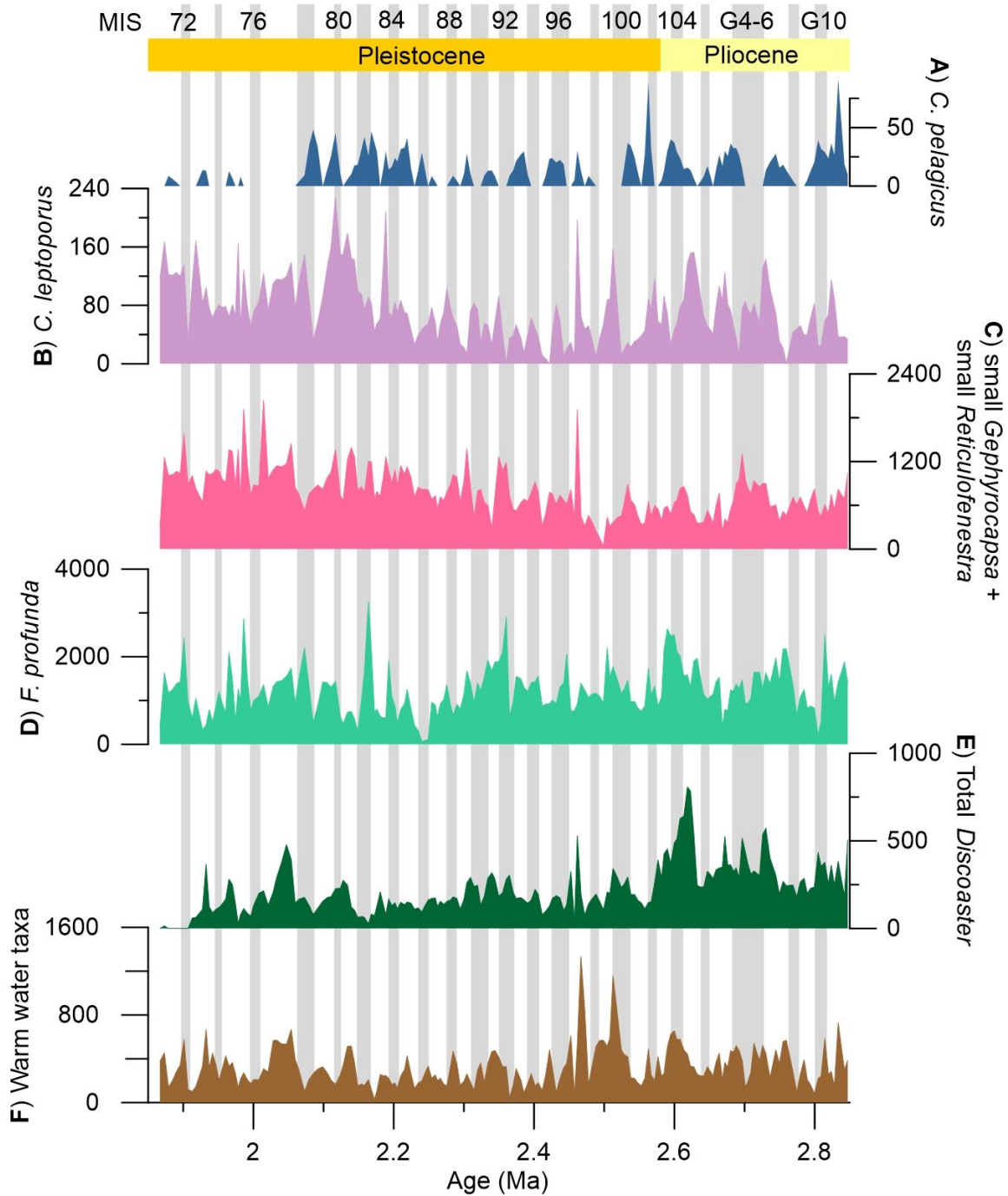
Figure 6: Absolute concentrations of selected calcareous nannofossil taxa: (**A**) *Coccolithus pelagicus*; (**B**) *Calcidiscus leptoporus*; (**C**) small *Gephyrocapsa* + small *Reticulofenestra*; (**D**) *Florisphaera profunda*; (**E**) total *Discoaster* spp.; (**F**) warm water taxa comprising *Oolithotus* spp., *Rhabdosphaera clavigera*, *Syracosphaera* spp., and *Umbellosphaera* spp. All concentrations are expressed in number of nannofossils x 10⁹/gram of sediment. Glacial stages are marked by gray bars.

479

480

481

482

5.3 Response of calcareous nannoplankton to astronomical forcing

Calcareous nannoplankton abundances visually exhibit cyclic variations (**Fig. 5** and **6**), which is confirmed by spectral analysis (**Fig. 7**). Spectral analysis performed on the nannofossil record demonstrates variations in paleoproductivity related to glacial/interglacial variability (100 kyr), obliquity (41 kyr) and precession (23 and 19 kyr). The nannofossil warm water taxa group, estimated primary productivity, and *F. profunda* index also show variations at the sub-precession and precession band (19 and 23 kyr). This strongly suggests that productivity in the Mozambique Channel is modulated by both the high latitude and the tropical Pacific forcings. The 100-kyr and obliquity signatures suggest a NH driver of the observed variability, whereas variability at the rhythm of precession is interpreted as a tropical Pacific forcing. The 23 kyr cyclicity in the calcareous nannofossil record from this site was also observed in the equatorial Indian Ocean, which was linked to a combination of both the boreal monsoon and the El Niño Southern Oscillation (ENSO)-like dynamics (Beaufort et al., 2001).
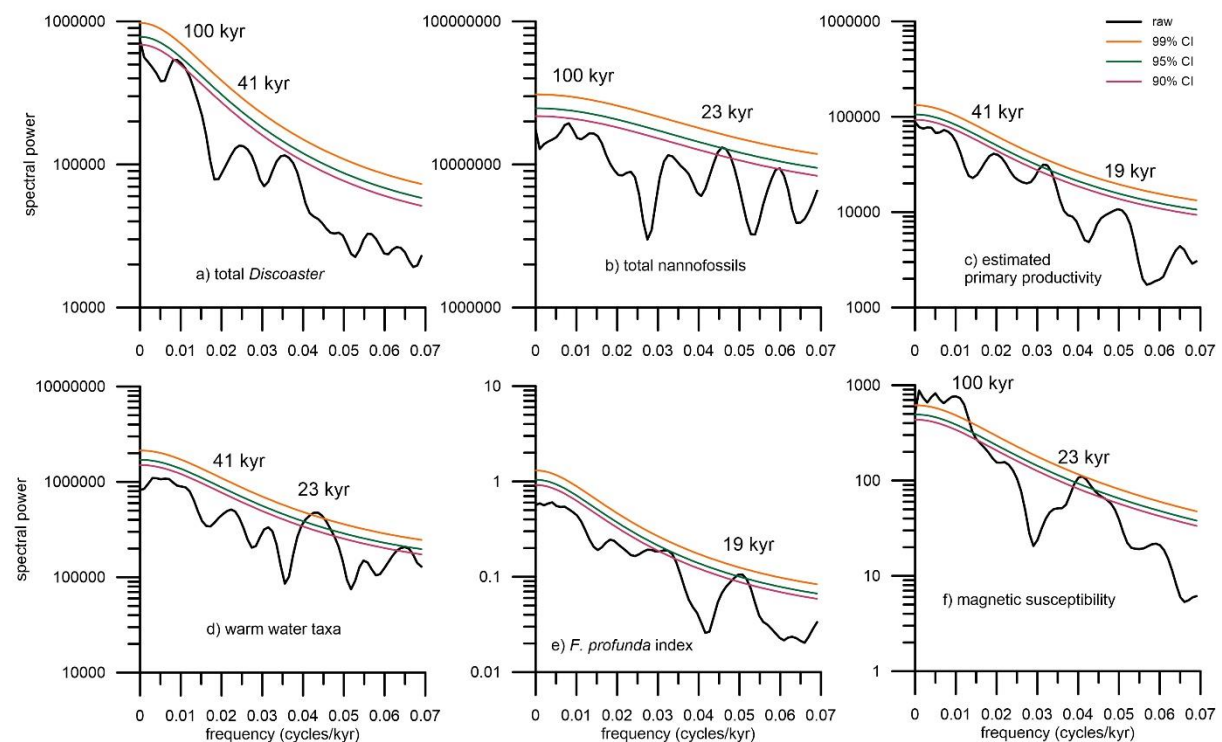
Figure 7: Spectral power versus frequency plots of calcareous nannoplankton record and magnetic susceptibility: (**A**) total *Discoaster* species; (**B**) total nannofossils; (**C**) estimated primary productivity calculated from relative abundance of *Florisphaera profunda*; (**D**) warm water taxa (*Oolithotus* spp., *Rhabdosphaera clavigera*, and *Syracosphaera* spp.); (**E**) *F. profunda* index; (**F**) magnetic susceptibility. Colored lines indicate the 90%, 95%, and 99% confidence intervals (CI).

5.4 Implications for the Agulhas Current

We suggest that the long-term record of paleoproductivity at Site U1476 is driven by both atmospheric and oceanographic processes, which influenced variations in the nutricline/thermocline dynamics and nutrient availability in the water column. The present day oceanography of the western Indian Ocean has been suggested to be linked to the Pacific Ocean climate variability (Schouten et al., 2003) and also holds true for Quaternary climate archives (Kuhnert et al., 2014; Tangunan et al., 2017). The abundance of the LPZ-dwelling species *F. profunda* is an effective proxy for the nutricline/thermocline depth in Quaternary sediments and has proven useful for late Neogene sequences (Okada, 2000), as well as for interpreting Indo-Pacific teleconnections over the past 300 kyr (Tangunan et al., 2017). The regular occurrence of warm water taxa reflects tropical Pacific influence in our study area. This shows that the transport of warm and oligotrophic surface water of the ITF via the SEC across the Indian Ocean was a persistent feature of the last 2.85 Myr, which could be linked to the development of the Agulhas Current downstream, and subsequent leakage into the South Atlantic (Biastoch et al., 2009).

A possible influence of southern sourced waters at Site U1476 is shown by the increase in the abundance of *C. pelagicus*. This species was not encountered in late Quaternary sediments of the equatorial Indian Ocean (Tangunan et al., 2017) but was found in the subtropical region of the Indian Ocean (e.g., Flores et al., 1999), which could be attributed to the influence of nutrient-rich SASW during the glacial periods, with the northward migration of the subtropical front (STF). However, the STF did not migrate northward beyond 33˚S during the glacial periods (Bard and Rickaby, 2009) and did not reach our study site in the Mozambique Channel. This region has been described by Ternon et al. (2014) as one of the most turbulent areas in the world oceans. Enhanced surface water productivity and cooler water conditions resulting in the occurrences of these species could therefore also be due to a localized upwelling event, hence intensified water column mixing driven by the mesoscale anticyclonic eddies in the channel (Schouten et al., 2003).

6 Conclusions

The Plio-Pleistocene paleoenvironment reconstruction over the last 1 Myr prior to the *Discoaster* extinction at Site U1476, using calcareous nannoplankton assemblage proxies showed that:

1. Global extreme climatic shift during the Plio-Pleistocene transition played a key role in the nutricline and thermocline depths, and thus the nutrient availability at the

Mozambique Channel. Both temperature and nutrient availability are critical parameters in calcareous nannoplankton productivity at the location.

2. Calcareous nannoplankton taxa exhibit periodic variability at pace with the astronomical parameters. The 100-kyr and obliquity signatures suggest a NH driver of the observed variability, whereas variability at the rhythm of precession is interpreted as a tropical Pacific forcing.

3. Discoasters at Site U1476 declined with global cooling across the Plio-Pleistocene, which resulted in reduced water column stratification and consequent shallowing of the nutricline/thermocline, hence high surface water productivity. We propose that the gradual decline and successive extinction of this group is due to a more mixed water column and consequent increase in productivity at the location, as shown by the low values of the *F. profunda* index and high abundances of UPZ flora, indicative of intensified water column mixing and nutrient-rich surface water conditions, respectively.

4. The transport of warm and oligotrophic surface water of the ITF via the SEC across the Indian Ocean was a persistent feature of the last 2.85 Myr, observed from the consistent occurrences of warm water taxa. A possible influence of the southern sourced sub-Antarctic surface waters into the site exists as shown by the increase in abundance of *C. pelagicus,* a species that is adapted to cold and high-nutrient environments.

Acknowledgments

References

Acker, J.G. & Leptoukh, G. 2007. Online analysis enhances use of NASA earth science data. *Eos, Transactions American Geophysical Union*, 88(2): 14-17.

Agnini, C., Monechi, S. & Raffi, I. 2017. Calcareous nannofossil biostratigraphy: historical background and application in Cenozoic chronostratigraphy. *Lethaia*, 50(3): 447-463.

Ahagon, N., Tanaka, Y. & Ujiie, H. 1993. Florisphaera profunda, a possible nannoplankton indicator of late Quaternary changes in sea-water turbidity at the northwestern margin of the Pacific, *Marine Micropaleontology*: 255-273.

Antoine, D. & Morel, A. 1996. Oceanic primary production: 1. Adaptation of a spectral light-photosynthesis model in view of application to satellite chlorophyll observations, *Global Biogeochemical Cycles*: 43-55.

Aubry, M.-P. 1998. Early Paleogene calcareous nannoplankton evolution: a tale of climatic amelioration. *Late Paleocene-Early Eocene climatic and biotic events in the marine and terrestrial records.* Columbia University Press, New York: 158-203.

Aubry, M.-P. 2007. A major Pliocene coccolithophore turnover: Change in morphological strategy in the photic zone. *Geological Society of America Special Papers*, 424: 25-51.

Backman, J. & Pestiaux, P. 1987. Pliocene Discoaster abundance variations, Deep Sea Drilling Project Site 606: Biochronology and palaeoenvironmental implications. *Ruddiman, W.E., Kidd, R.B., Thomas, E., et al., Initial Reports of the Deep Sea Drilling Project*, 94: 903-909.

Bard, E. & Rickaby, R.E. 2009. Migration of the subtropical front as a modulator of glacial climate, *Nature*: 380-383.

Baumann, K.H., Andruleit, H.A. & Samtleben, C. 2000. Coccolithophores in the Nordic Seas: comparison of living communities with surface sediment assemblages. *Deep-Sea Research Part Ii-Topical Studies in Oceanography*, 47(9-11): 1743-1772.

Baumann, K.H. & Freitag, T. 2004. Pleistocene fluctuations in the northern Benguela Current system as revealed by coccolith assemblages, *Mar Micropaleontol*: 195-215.

Beal, L.M., Ruijter, W.P.M.D., Biastoch, A., Zahn, R. & 136, S.W.I.W.G. 2011. On the role of the Agulhas system in ocean circulation and climate. *Nature*, 472: 429-436.

Beaufort, L. 1996. Dynamics of the monsoon in the equatorial Indian Ocean over the last 260,000 years, *Quaternary International*: 13-18.

Beaufort, L., De Garidel-Thoron, T., Mix, A.C. & Pisias, N.G. 2001. ENSO-like forcing on oceanic primary production during the Late Pleistocene, *Science*. American Association for the Advancement of Science: 2440-2444.

Beaufort, L., Lancelot, Y., Camberlin, P.C., O., Vincent, E., Bassinot, F.C. & Labeyrie, L. 1997. Insolation cycles as a major control of equatorial Indian Ocean primary production, *Science*: 1451-1454.

Berger, A. 1992. Orbital variations and insolation database. *IGBP PAGES/World Data Center-A for Paleoclimatology Data Contribution Series*, 92(007).

Berggren, W. A., Hilgen, F. J., Langereis, C. G., Kent, D. V., Obradovich, J. D., Raffi, I., Raymo, M.E. & Shackleton, N. J. 1995. Late Neogene chronology: new perspectives in high-resolution stratigraphy. *Geological Society of America Bulletin*, *107*(11), 1272-1287.

Biastoch, A., Böning, C.W., Schwarzkopf, F.U. & Lutjeharms, J. 2009. Increase in Agulhas leakage due to poleward shift of Southern Hemisphere westerlies. *Nature*, 462(7272): 495-498.

Bolton, C. T., Lawrence, K. T., Gibbs, S. J., Wilson, P. A., & Herbert, T. D. 2011. Biotic and geochemical evidence for a global latitudinal shift in ocean biogeochemistry and export productivity during the late Pliocene. *Earth and Planetary Science Letters*, *308*(1), 200-210.

Bordiga, M., Bartol, M. & Henderiks, J. 2015. Absolute nannofossil abundance estimates: Quantifying the pros and cons of different techniques. *Revue de micropaléontologie*, 58(3): 155-165.

632   Bown, P.R., Lees, J.A. & Young, J.R. 2004. Calcareous nannoplankton evolution and diversity
633   through time*, Coccolithophores.* Springer: 481-508.
634   Bralower, T.J. 2002. Evidence of surface water oligotrophy during the Paleocene-Eocene
635   thermal maximum: Nannofossil assemblage data from Ocean Drilling Program Site
636   690, Maud Rise, Weddell Sea. *Paleoceanography*, 17(2).
637   Browning, E., Bergen, J., Blair, S., Boesiger, T. & E. de Kaenel. 2017. Late Miocene to Late
638   Pliocene taxonomy and stratigraphy of the genus *Discoaster* in the circum North
639   Atlantic Basin: Gulf of Mexico and ODP Leg 154. *Journal of Nannoplankton Research*,
640   37(2-3), 189-214.
641   Bukry, D. 1971. Discoaster evolutionary trends. *Micropaleontology*: 43-52.
642   Chapman, M.R. & Chepstow-Lusty, A.J. 1997. Late Pliocene climatic change and the global
643   extinction of the discoasters: an independent assessment using oxygen isotope
644   records. *Palaeogeography, Palaeoclimatology, Palaeoecology*, 134(1): 109-125.
645   Chepstow-Lusty, A., Backman, J. & Shackleton, N.J. 1989. Comparison of upper Pliocene
646   Discoaster abundance variations from North Atlantic Sites 552, 607, 658, 659 and 662:
647   further evidence for marine plankton responding to orbital forcing, *Ruddiman, W.F.,*
648   *Sarnthein, M., et al., Proceedings of the ODP, Science Results*: 121-141.
649   Christensen, B.A., Renema, W., Henderiks, J., De Vleeschouwer, D., Groeneveld, J.,
650   Castañeda, I.S., Reuning, L., Bogus, K., Auer, G., Ishiwa, T. & McHugh, C.M. 2017.
651   Indonesian Throughflow drove Australian climate from humid Pliocene to arid
652   Pleistocene. *Geophysical Research Letters.* 44(*13*), 6914–6925.
653   Clemens, S.C., Murray, D.W. & Prell, W.L. 1996. Nonstationary phase of the Plio-Pleistocene
654   Asian monsoon. *Science*, 274(5289): 943.
655   Demenocal, P. B. 1995. Plio-Pleistocene African climate. *Science*, 53-59.
656   De Vleeschouwer, D., Vahlenkamp, M., Crucifix, M., & Pälike, H. 2017. Alternating Southern
657   and Northern Hemisphere climate response to astronomical forcing during the past 35
658   my. *Geology*, *45*(4), 375-378.
659   Flores, J.A., Sierro, F.J. & Raffi, I., 1995. Evolution of the calcareous nannofossil assemblage
660   as a response to the paleoceanographic changes in the eastern equatorial Pacific
661   Ocean from 4 to 2 Ma (Leg 138, Sites 849 and 852). *In Proceedings of the ODP,*
662   *Science* Results, 138:163-176. Ocean Drill. Prog College Station, TX.
663   Flores, J.A., Gersonde, R. & Sierro, F.J. 1999. Pleistocene fluctuations in the Agulhas Current
664   Retroflection based on the calcareous plankton record, *Marine Micropaleontology*: 1-
665   22.
666   Friedinger, P.J. & Winter, A. 1987. Distribution of modern coccolithophore assemblages in the
667   southwest Indian Ocean off southern Africa. *Journal of Micropalaeontology*, 6(1): 49-
668   56.
669   Gibbs, S., Shackleton, N. & Young, J. 2004. Orbitally forced climate signals in mid-Pliocene
670   nannofossil assemblages. *Marine Micropaleontology*, 51(1-2): 39-56.
671   Giraudeau, J. 1992. Distribution of Recent nannofossils beneath the Benguela System -
672   Southwest African continental margin, *Marine Geology*: 219-237.
673   Gradstein, F.M., Ogg, G. & Schmitz, M. 2012. *The Geologic Time Scale 2012*, 117. Elsevier:
674   6 pp.
675   Hall, I.R., Hemming, S.R. & Levay, L.J. 2016. Expedition 361 Preliminary Report: South
676   African Climates (Agulhas LGM Density Profile). International Ocean Discovery
677   Program.
678   Hall, I.R., Hemming, S.R., Levay, L.J., Barker, S., Berke, M.A., Brentegani, L., Caley, T.,
679   Cartagena-Sierra, A., Charles, C.D., Coenen, J.J., Crespin, J.G., Franzese, A.M.,
680   Gruetzner, J., Han, X., Hines, S.K.V., Jimenez Espejo, F.J., Just, J., Koutsodendris,
681   A., Kubota, K., Lathika, N., Norris, R.D., Periera Dos Santos, T., Robinson, R.,
682   Rolinson, J.M., Simon, M., Tangunan, D., Van Der Lubbe, J.J.L., Yamane, M. & Zhang,
683   H. 2017a. Expedition 361 methods. *In*: I. R. Hall, Hemming, S.R., LeVay, L.J., and the
684   Expedition 361 Scientists (Ed.)*, South African Climates (Agulhas LGM Density Profile).*
685   International Ocean Discovery Program.

Hall, I.R., Hemming, S.R., Levay, L.J., Barker, S., Berke, M.A., Brentegani, L., Caley, T., Cartagena-Sierra, A., Charles, C.D., Coenen, J.J., Crespin, J.G., Franzese, A.M., Gruetzner, J., Han, X., Hines, S.K.V., Jimenez Espejo, F.J., Just, J., Koutsodendris, A., Kubota, K., Lathika, N., Norris, R.D., Periera Dos Santos, T., Robinson, R., Rolinson, J.M., Simon, M., Tangunan, D., Van Der Lubbe, J.J.L., Yamane, M. & Zhang, H. 2017b. Site U1476. *In*: I. R. Hall, Hemming, S.R., LeVay, L.J., and the Expedition 361 Scientists (Ed.)*, South African Climates (Agulhas LGM Density Profile)*. International Ocean Discovery Program.

Hammer, Ø., Harper, D. & Ryan, P. 2009. PAST-PAlaeontological STatistics, ver. 1.89, *University of Oslo, Oslo*: 1-31.

Haq, B.U. & Lohmann, G. 1976. Early Cenozoic calcareous nannoplankton biogeography of the Atlantic Ocean. *Marine Micropaleontology*, 1: 119-194.

Hastenrath, S., Nicklis, A. & Greischar, L. 1993. Atmospheric-hydrospheric mechanisms of climate anomalies in the western equatorial Indian Ocean. *Journal of Geophysical Research*, 98(C11): 20219.

Haug, G. H., D. M. Sigman, R. Tiedemann, T. F. Pedersen & Sarntheink, M. 1999. Onset of permanent stratification in the subarctic Pacific Ocean, *Nature*, 401(6755), 21–24.

Hine, N. & Weaver, P.P.E. 1998. Quaternary. *Calcareous nannofossil biostratigraphy*, 266-283.

Kuhnert, H., Kuhlmann, H., Mohtadi, M., Meggers, H., Baumann, K.H. & Patzold, J. 2014. Holocene tropical western Indian Ocean sea surface temperatures in covariation with climatic changes in the Indonesian region, *Paleoceanography*: 423-437.

Lawrence, K.T., Sigman, D., Herbert, T.D., Riihimaki, C., Bolton, C., Martinez-Garcia, A., Rosell-Mele, A. & Haug, G. 2013. Time-transgressive North Atlantic productivity changes upon Northern Hemisphere glaciation. *Paleoceanography*, 28(4): 740-751.

Lisiecki, L.E. & Raymo, M.E. 2005. A Pliocene-Pleistocene stack of 57 globally distributed benthic δ18O records. *Paleoceanography*, 20(1): n/a-n/a.

Lourens, L., Hilgen, F., Shackleton, N.J., Laskar, J., and Wilson, D., 2004. The Neogene period. In Gradstein, F.M., Ogg, J.G., and Smith, A. (Eds.), A Geologic Time Scale 2004: Cambridge, United Kingdom (Cambridge University Press), 409–440.

Lutjeharms, J. 2006. The agulhas current. *African Journal of Marine Science*, 28(3-4): 729-732.

Marino, M., Maiorano, P. & Flower, B.P. 2011. Calcareous nannofossil changes during the Mid-Pleistocene Revolution: Paleoecologic and paleoceanographic evidence from North Atlantic Site 980/981. *Palaeogeography Palaeoclimatology Palaeoecology*, 306(1-2): 58-69.

Marino, M., Maiorano, P., Tarantino, F., Voelker, A., Capotondi, L., Girone, A., Lirer, F., Flores, J.-A. & Naafs, B.D.A. 2014. Coccolithophores as proxy of seawater changes at orbital-to-millennial scale during middle Pleistocene Marine Isotope Stages 14-9 in North Atlantic core MD01-2446. *Paleoceanography*, 29(6): 518-532.

Martini, E. 1971. Standard Tertiary and Quaternary calcareous nannoplankton zonation, *Proceedings of the Second Planktonic Conference, Roma 1970*. Tecnoscienza: 739-785.

Minoletti, F., Gardin, S., Nicot, E., Renard, M. and Spezzaferri, S., 2001. Mise au point d'un protocole experimental de separation granulometrique d'assemblages de nannofossiles calcaires; applications paleoecologiques et geochimiques, *Bulletin de la Société géologique de France*, 172(4): 437-446.

Molfino, B. & Mcintyre, A. 1990. Precessional forcing of nutricline dynamics in the equatorial atlantic, *Science*. American Association for the Advancement of Science: 766-769.

Okada, H. 2000. 33. Neogene and Quaternary calcareous nannofossils from the Blake Ridge, Sites 994, 995, AND 9971, *Proceedings of the Ocean Drilling Program. Scientific results*. Ocean Drilling Program: 331-341.

Okada, H. & Bukry, D. 1980. Supplementary modification and introduction of code numbers to the low-latitude coccolith biostratigraphic zonation (Bukry, 1973; 1975). *Marine Micropaleontology*, 5: 321-325.

Parente, A., Cachao, M., Baumann, K.H., De Abreu, L. & Ferreira, J. 2004. Morphometry of Coccolithus pelagicus s.l. (Coccolithophore, Haptophyta) from offshore Portugal, during the last 200 ka. *Micropaleontology*, 50: 107-120.

Perch-Nielsen, K. 1985. Cenozoic calcareous nannofossils. *Plankton stratigraphy*, 427-554.

Raffi, I., Backman, J., Fornaciari, E., Pälike, H., Rio, D., Lourens, L. & Hilgen, F. 2006. A review of calcareous nannofossil astrobiochronology encompassing the past 25 million years. *Quaternary Science Reviews*, 25(23): 3113-3137.

Ravelo, A.C., Andreasen, D.H., Mitchell, L., Lyle, A.O. & Wara, M.W. 2004. Regional climate shifts caused by gradual global cooling in the Pliocene epoch. *Nature*, 429(6989): 263.

Raymo, M., Hodell, D. & Jansen, E. 1992. Response of deep ocean circulation to initiation of Northern Hemisphere glaciation (3–2 Ma). *Paleoceanography*, 7(5): 645-672.

Rio, D., Raffi, I., & Villa, G. (1990). Pliocene-Pleistocene calcareous nannofossil distribution patterns in the Western Mediterranean. In *Proceedings of the Ocean Drilling Program, Scientific Results* (Vol. 107, pp. 513-533). College Station, TX: Ocean Drilling Program.

Rogalla, U. & Andruleit, H. 2005. Precessional forcing of coccolithophore assemblages in the northern Arabian Sea: Implications for monsoonal dynamics during the last 200,000 years, *Marine Geology*: 31-48.

Sarnthein, M., & Fenner, J. 1988. Global Wind-Induced Change of Deep-Sea Sediment Budgets, New Ocean Production and CO $ _2 $ Reservoirs ca. 3.3-2.35 Ma BP. *Philosophical Transactions of the Royal Society of London B: Biological Sciences*, 318(1191), 487-504.

Schott, F.A. & Mccreary, J.P. 2001. The monsoon circulation of the Indian Ocean, *Progress in Oceanography*. Progress in Oceanography: 1-123.

Schott, F.A., Xie, S.P. & Mccreary, J.P. 2009. Indian Ocean circulation and climate variability, *Rev Geophys*.

Schouten, M.W., De Ruijter, W.P.M., Van Leeuwen, P.J. & Ridderinkhof, H. 2003. Eddies and variability in the Mozambique Channel, *Deep-Sea Research Part Ii-Topical Studies in Oceanography*: 1987-2003.

Schueth, J.D. & Bralower, T.J. 2015. The relationship between environmental change and the extinction of the nannoplankton Discoaster in the early Pleistocene. *Paleoceanography*, 30(7): 863-876.

Shackleton, N.J., Backman, J., Zimmerman, H.T., Kent, D.V., Hall, M., Roberts, D.G., Schnitker, D., Baldauf, J., Desprairies, A. & Homrighausen, R. 1984. Oxygen isotope calibration of the onset of ice-rafting and history of glaciation in the North Atlantic region. *Nature*, 307(5952): 620-623.

Simpson, E. & Schlich, R. 1974. Initial reports of the Deep Sea Drilling Project, vol. 25. *Washington, DC: US Government Printing Office*.

Stolz, K., Baumann, K.-H. & Mersmeyer, H. 2015. Extant coccolithophores from the western equatorial Indian Ocean off Tanzania and coccolith distribution in surface sediments, *Micropaleontology*: 473-488.

Tangunan, D., Baumann, K.-H., Pätzold, J., Henrich, R., Kucera, M., De Pol-Holz, R. & Groeneveld, J. 2017. Insolation forcing of coccolithophore productivity in the western tropical Indian Ocean over the last two glacial-interglacial cycles. *Paleoceanography*.

Ternon, J.F., Bach, P., Barlow, R., Huggett, J., Jaquemet, S., Marsac, F., Menard, F., Penven, P., Pontier, M. & Roberts, M.J. 2014. The Mozambique Channel: From physics to upper trophic levels. *Deep Sea Research Part II: Tropical Studies in Oceanography*, 100: 9.

Tiedemann, R., Sarnthein, M., & Shackleton, N. J. 1994. Astronomic timescale for the Pliocene Atlantic δ18O and dust flux records of Ocean Drilling Program Site 659. *Paleoceanography*, 9(4), 619-638.

Westbroek, P., Brown, C. W., van Bleijswijk, J., Brownlee, C., Brummer, G. J., Conte, M., Egge, J., Fernandez, E., Jordan, R., Knappertsbusch, M. & Stefels, J. (1993). A model system approach to biological climate forcing. The example of Emiliania huxleyi. *Global and Planetary Change*, 8(1-2), 27-46.

796   Winter, A., Jordan, R.W. & Roth, P.H. 1994. Biogeography of living coccolithophores in ocean
797   waters. *In*: A. Winter & W. G. Siesser (Eds.)*, Coccolithophores*. Cambridge University
798   Press: 37.
799   Winter, A. & Martin, K. 1990. Late Quaternary history of the Agulhas Current,
800   *Paleoceanography*: 479-486.
801   Young, J.R. 1998. Neogene. *Calcareous nannofossil biostratigraphy*, 225-265.

Supplementary materials for "The last 1 million years of the extinct genus *Discoaster*: Plio–Pleistocene environment and productivity at Site U1476 (Mozambique Channel)"

Deborah N. Tangunan[a], Karl-Heinz Baumann[a,b], Janna Just[b], Leah J. LeVay[c], Stephen Barker[d], Luna Brentegani[e], David De Vleeschouwer[a], Ian R. Hall[d], Sidney Hemming[f], Richard Norris[g] and the Expedition 361 Shipboard Scientific Party[10]

This PDF file includes:

- Expedition 361 Shipboard Scientific Party
- Supplementary information for the age model construction.
    - Fig. S1. Application of bandpass filter and astronomical calibration of the Site U1476 XRF Fe/Ca data series.
    - Fig. S2. Inclination of shipboard core-half measurements for Site U1476 holes A, D and E.
    - Table S1. Calcareous nannofossil biostratigraphic events recorded at Site U1476 with the astronomically calibrated occurrences of the index taxa.
   - Table S2. Paleomagnetic boundaries at Site U1476.

Expedition 361 Shipboard Scientific Party

Melissa A. Berke[h], Thibaut Caley[i], Alejandra Cartagena-Sierra[h], Christopher D. Charles[g], Jason J. Coenen[j], Julien G. Crespin[i], Allison M. Franzese[k], Jens Gruetzner[l], Xibin Han[m], Sophia K.V. Hines[n], Francisco J. Jimenez Espejo[o], Andreas Koutsodendris[p], Kaoru Kubota[q], Nambiyathodi Lathika[r], Thiago Pereira dos Santos[s], Rebecca Robinson[t], John M. Rolison[u], Margit H. Simon[v], Jeroen J.L. van der Lubbe[w], Masako Yamane[x], and Hucai Zhang[y].

[h]Department of Civil Engineering & Geological Sciences, University of Notre Dame, 156 Fitzpatrick Hall, Notre Dame IN 46556, USA; [i]EPOC, UMR CNRS 5805, University of Bordeaux, Allee Geoffroy Saint Hilaire, Pessac 33615, France; [j]Department of Geology, Northern Illinois University, 235 N. Sacramento Street, Unit F, Sycamore IL 60178, USA; [k]Natural Sciences Department, School of Earth and Environmental Sciences, Hostos Community College, 500 Grand Concourse, Bronx NY 10451, USA; [l]Alfred-Wegener-Institut for Polar and Marine Research, Am Alten Hafen 26, Bremerhaven 27568 Germany; [m]Second Institute of Oceanography, Key Laboratory of Submarine Science, 36 Baochubeilu, Hangzhou City, P.R. China; [n]Division of Geological and Planetary Sciences, California Institute of Technology, 1200 E. California Boulevard, MC 131-24, Pasadena CA 91125, USA; [o]Institute of Biogeosciences, Japan Agency for Marine-Earth Science and Technology (JAMSTEC), Natsushima-cho 2-15, Yokosuka 237-0061, Japan; [p]Institute of Earth Sciences, University of Heidelberg, Im Neuenheimer Feld 234, Heidelberg 69120; [q]Atmosphere and Ocean Research Institute, University of Tokyo, 5-1-5 Kashiwano-ha, Kashiwashi Chiba 277-8564, Japan; [r]Ice Core Laboratory, National Centre for Antarctic and Ocean Research, Head Land Sada, Vasco da Gama Goa 403804, India; [s]Institute for Geosciences, Universidade Federal Fluminense, Rio de Janeiro 24020, Brazil; [t]Graduate School of Oceanography, University of Rhode Island, South Ferry Road, Narragansett RI 02882, USA; [u]Chemistry Department, University of Otago, PO Box 56, Dunedin 9054, New Zealand; [v]Uni Research Climate and Bjerknes Centre for Climate Research, Allégt. 55, 5007 Bergen, Norway; [w]Department of Sedimentology, University Amsterdam, Netherlands; [x]Department of Biogeochemistry, JAMSTEC, 2-15 Natsushima-cho, Yokosuka, Kanagawa 237-0061, Japan; [y]Lab of Plateau Lake Ecology and Global Change, Yunnan Normal University, 1 Yuhua District, Kunming Chengong 650500, P.R. China.

Supplementary information for the age model construction

The Site U1476 Plio-Pleistocene (2.85 to 1.85 Myr) age model was established based on the combined calcareous nannofossil biostratigraphy, magnetostratigraphy and cyclostratigraphy.
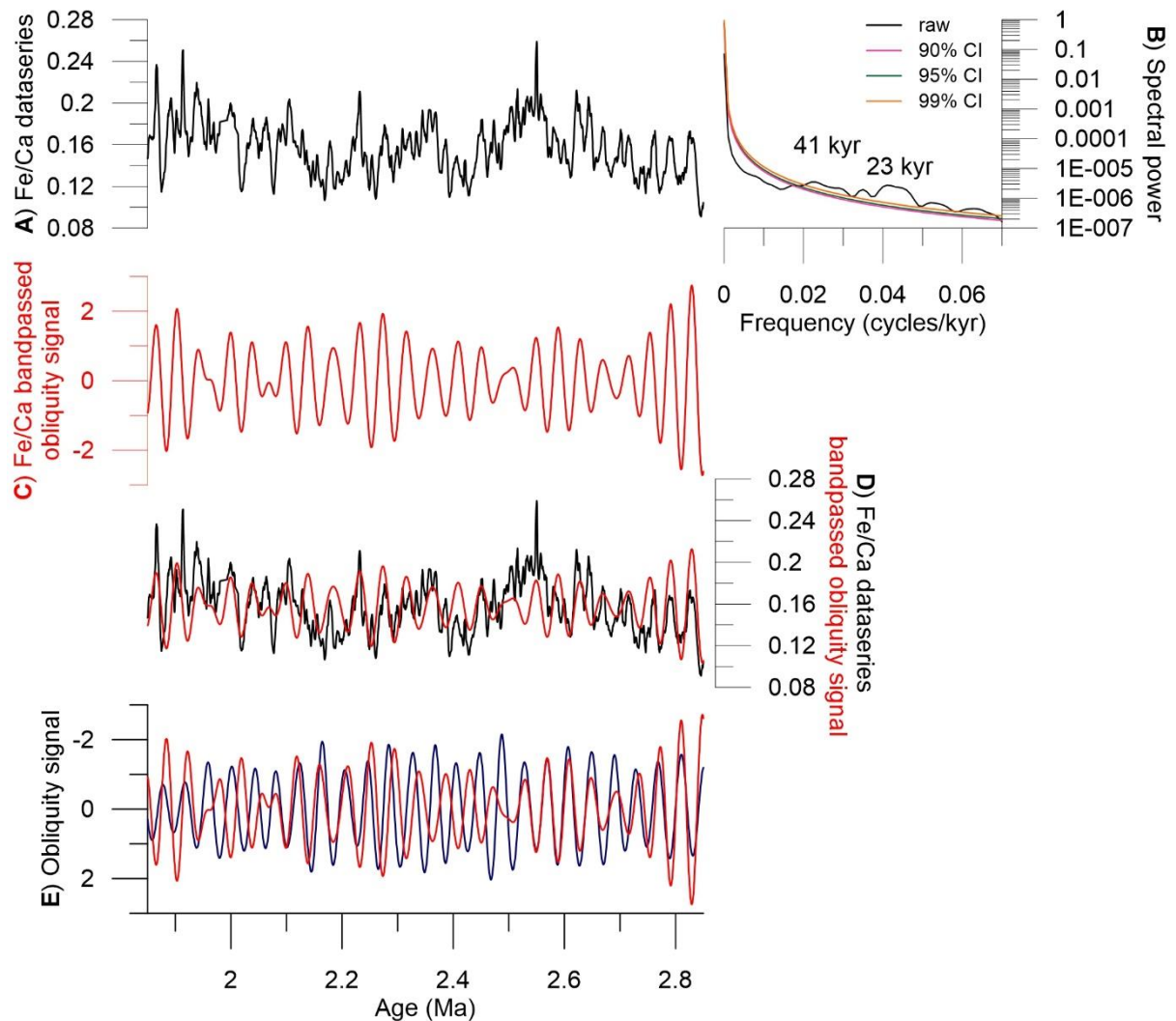
Figure S1: Application of bandpass filter and tuning of the Site U1476 XRF Fe/Ca data series to La2010 astronomical solution by Laskar, (2011): **A**) Fe/Ca record plotted against the shipboard stratigraphy; **B**) power spectra of the Fe/Ca data to determine orbital imprint in the record; **C**) band passed 41-kyr obliquity signal filtered in the Fe/Ca data; **D**) visual comparison of the Fe/Ca data series and the filtered obliquity signal; and **E**) Site U1476 Fe/Ca filtered obliquity signal plotted with the La2010 obliquity solution.

107 **Table S1:** Calcareous nannofossil biostratigraphic events recorded at Site U1476 with the astronomically calibrated occurrences of the index taxa in the
108 Mozambique Channel, western Indian Ocean.
109

Calcareous nannofossil event	Age (Ma) Gradstein et al., 2012)	SHIPBOARD		CALIBRATED: Splice		
		Hole-Core-Section-interval	CCSF (m)	Hole-Core-Section-interval	CCSF (m)	Age (Ma) THIS STUDY
T *C. macintyrei*	1.60	U1476A-5H2-75 cm	36.63			
B *Gephyrocapsa* (>4µm)	1.73	U1476A-5H2-75 cm	41.13			
T *D. brouweri*	1.93	U1476A-6H2-75 cm	46.06	U1476D-6H5-81 cm	45.29	1.91
T *D. triradiatus*	1.95	U1476A-6H2-75 cm	46.06	U1476D-6H5-141 cm	45.89	1.93
Bc *D. triradiatus*	2.14	U1476A-6H6-60 cm	51.91	U1476E-6H3-147 cm	51.08	2.13
T *D. pentaradiatus*	2.39	U1476A-7H6-75 cm	61.64	U1476A-7H5-108 cm	60.97	2.45
T *D. surculus*	2.49	U1476A-8H1-75 cm	64.31	U1476D-8H4-125 cm	63.42	2.53
T *D. tamalis*	2.80	U1476A-8H6-75 cm	71.81	U1476D-9H4-6 cm	72.72	2.81
T *Sphenolithus* spp.	3.54	U1476A-11H6-75 cm	103.13			

110

Table S2: Paleomagnetic boundaries at Site U1476. The most reliable paleomagnetic boundaries are marked by an asterisk.

Boundary	Age (Ma) GPTS 2012	Hole-Core-Section-interval	CCSF (m)	Hole-Core-Section-interval	CCSF (m)	Age (Ma) THIS STUDY
B Jaramillo	1.07	U1476D-4H5-68 cm	26.49*	U1476E-3H6-67 cm	26.24	
T Olduvai	1.78	U1476D-6H2-64 cm	40.62	U1476E-5H2-110 cm	39.89*	
B Olduvai	1.95	U1476D-4H6-67 cm	46.65	U1476E-5H7-39 cm	46.28*	1.94
T Gauss	2.58	U1476D-8H7-34 cm	67.01	U1476E-*H2-107 cm	67.56*	2.66

Figure S2: Inclination of shipboard core-half measurements after 15 or 20 mT alternating field demagnetization (Hall et al. 2017b) for a) Hole A, b) Hole D and c) Hole E. As the paleomagnetic data from U1476 carry a strong coring overprint, in particular at the top of each core, data from the first sections of the cores are not shown. The depth of paleomagnetic polarity boundaries were defined by joint consideration of data from all holes.